

Final Technical Report

USGS Award 08HQGR0013

"DYNAMIC SIMULATION OF A M_w 7.0 EARTHQUAKE ON THE SIERRA MADRE FAULT SYSTEM AND ITS IMPLICATIONS FOR STRONG GROUND MOTION IN GREATER LOS ANGELES"

P.I. Gregory C. Beroza
Department of Geophysics
397 Panama Mall
Stanford, CA, 94305-2215

Phone: (650) 723-4958
Fax: (650) 725-7344
Email: beroza@stanford.edu

Research supported by the U.S. Geological Survey (USGS), Department of the Interior, under USGS award number 08-HQ-GR-0013. The views and conclusions contained in this document are those of the authors and should not be interpreted as necessarily representing the official policies, either expressed or implied, of the U.S. Government.

Technical Abstract

The Sierra Madre – Cucamonga fault system at the northern edge of the Los Angeles Basin, accommodates an important component of convergent motion across the southern Transverse Ranges and poses a significant seismic threat to metropolitan Los Angeles. In order to quantify the ground motion potential for a large earthquake on this reverse fault system, we model dynamically two M_w 7.7 scenario earthquakes by incorporating the non-planar dipping fault geometry from the SCEC community fault model and 3D crustal velocity structure from the SCEC Community Velocity Model in a finite-element code. The simulations uses ~ 1.2 billion elements and provides ground motion time histories in greater Los Angeles up to 0.5 Hz. Both the non-planar fault geometry and free surface have a significant effect on dynamic rupture propagation. We find that the near-fault ground motion reaches up to 7 m/s on the hanging wall. Ground motion in the Los Angeles basin is generally less than 1 m/s; however, in specific areas of the basin, ground motions can be as large as 3 m/s due to the basin-channeling effects, similar to the PGV distribution in some SCEC Terashake simulations. Both the up-dip and along-strike rupture directivity are not strong, as observed in recent large thrust earthquakes. Future work that incorporates the inelastic off-fault response during the dynamic rupture propagation, will modify the elastic ground motion estimates reported here.

Publications resulting from this grant include:

Ma, S. and G. C. Beroza (2009), Dynamic modeling of a hypothetical M_w 7.0 earthquake on the Sierra Madre fault system and resultant strong motions in greater Los Angeles, *Seism. Res. Lett.*, 80, 329.

Non-Technical Abstract

The Sierra Madre – Cucamonga fault system at the northern edge of Los Angeles Basin poses a significant seismic threat to metropolitan Los Angeles. Large earthquakes on this reverse fault system present a special concern because this densely populated area is in the forward direction of rupture propagation. We simulate dynamically two M_w 7.7 earthquake rupture scenarios by incorporating known non-planar fault geometry and 3D heterogeneous crustal velocity structures to provide the long-period ground motions expected in the greater Los Angeles area. Given our assumptions, we find that the ground motion near the fault can reach 7 m/s on the hanging wall. Ground motion in the Los Angeles basin is generally less than 1 m/s; however, in specific areas it can be as large as 3 m/s due to the propagation of seismic waves in heterogeneous velocity structures. The rupture directivity effect is not strong, similar to the observation in the 1999 Chi-Chi, Taiwan, earthquake and the 2008 Wenchuan, China, earthquake. These ground motion estimates (especially in the near-fault area) are based on elastic simulations and will likely be reduced once we include inelastic off-fault response. Our next step is to quantify the effect of the inelastic off-fault response on the earthquake rupture propagation and ground motion.

Dynamic Simulation of a M_w 7.0 Earthquake on the Sierra Madre Fault System and its Implication for Strong Ground Motion in Greater Los Angeles

Situated at the northern edge of the well-populated Los Angeles basin, the Sierra Madre and Cucamonga fault system (Figure 1) marks the abrupt change in topography at the southern flank of the San Gabriel Mountains and accommodates an important portion of convergent motion of southern Transverse Ranges. Paleoseismic studies (e.g., Dolan et al., 1995; Rubin et al., 1998) indicate that the Sierra Madre fault had ruptured at least twice in M 7.2 – 7.6 events in the past 15,000 years.

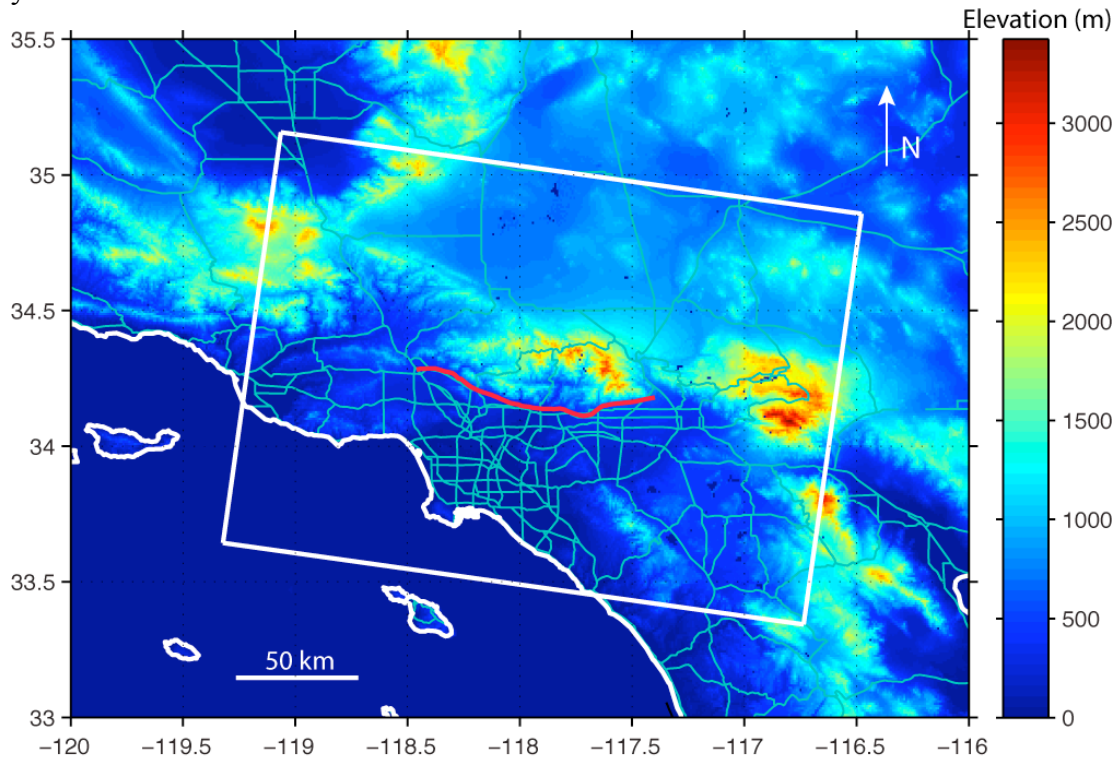


Figure 1. Topographic map of southern California. The trace of the Sierra Madre – Cucamonga Fault system is shown in red. White rectangle shows the area we include in the finite-element simulations. Major roads in the area are depicted in blue lines

In order to quantify the seismic hazard posed by the Sierra Madre – Cucamonga fault system, we have carried out elastic simulations for two M_w 7.7 scenario earthquakes using a finite-element method (Ma and Liu, 2006; Ma et al., 2008; Harris et al., 2009). We incorporated the non-planar geometry of the fault system (Figure 2) from the SCEC Community Fault Model (Plesch et al., 2007) and the 3D heterogeneous velocity structure from the SCEC Community Velocity Model 4.0 (Magistrale et al., 2000). The computational domain includes a 240 km x 170 km x 30 km volume in southern California (Figure 1). We used a structural finite element mesh with the element size of about 100 m everywhere, which resulted in about 1.2 billion elements – roughly the same computational size as the SCEC Terashake simulations (Olsen et al., 2008). We did not include the surface topography in the simulations. The minimum shear wave speed is 500 m/s, so the synthetic ground motions are accurate up to 0.5 Hz – the finite-element code requires about 10 nodes per minimum S-wave wavelength.

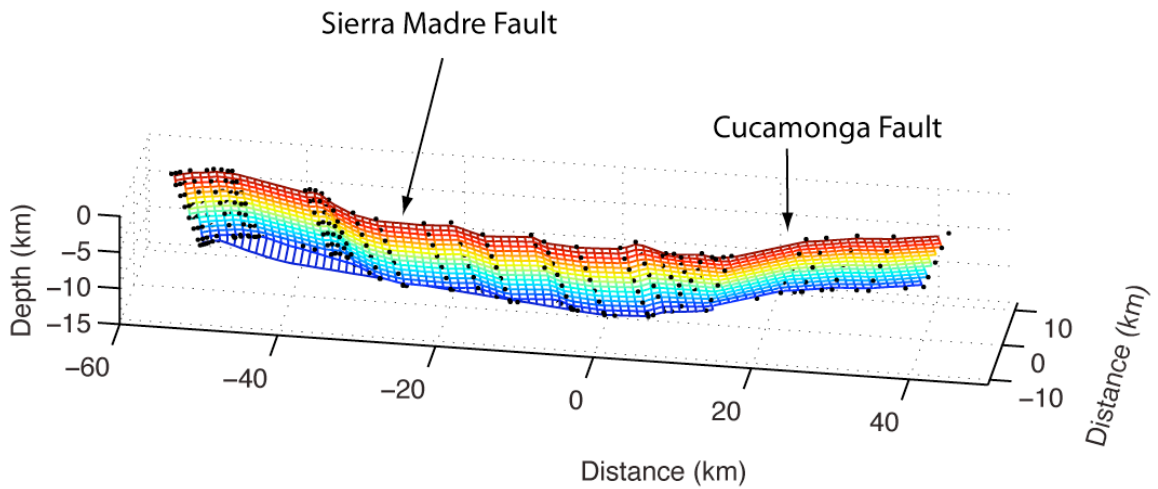


Figure 2. Geometry of the Sierra Madre – Cucamonga fault. The black dots are the defining points for the fault geometry in the SCEC Community Fault Model. A linear interpolation is used to generate the fault surface mesh.

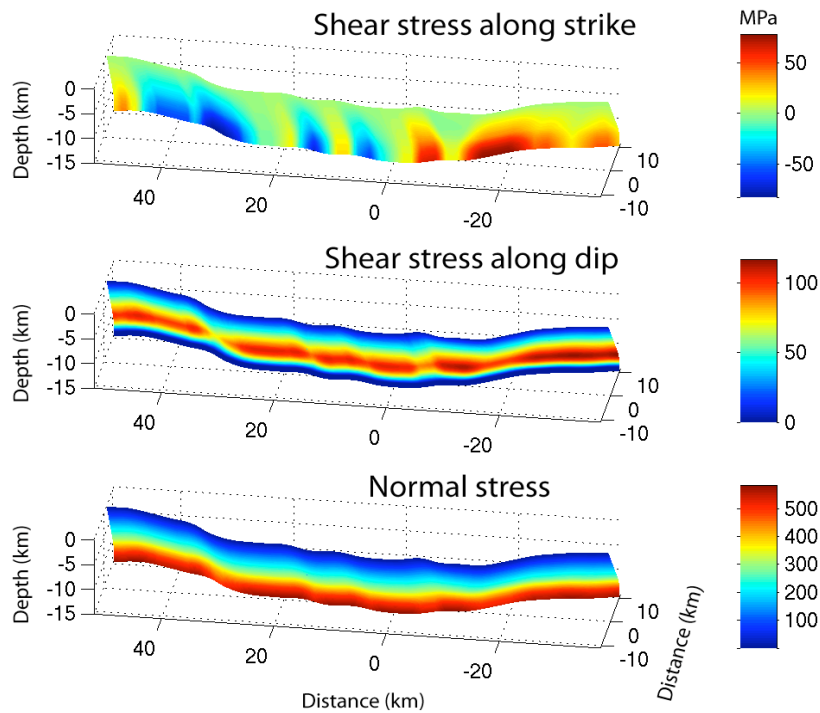


Figure 3. Initial stresses assumed in the simulations are mapped on the fault.

We assumed a simple stress environment in southern California. The maximum compressive stress, σ_1 , is N8°E and has a depth gradient 38.87 MPa/km and the minimum compressive stress, σ_3 , is vertical and the depth gradient is 16.66 MPa/km. The intermediate principal stress, σ_2 , is E8°S and has the relation $\sigma_2 = (\sigma_1 + \sigma_3)/2$. Note that all the stresses are depth-dependent. The initial stresses on the fault are obtained by resolving the three principal stresses onto the

nonplanar fault geometry, shown in Figure 3. Our assumption for the stress environment is consistent with existing stress measurements in southern California (Townend and Zoback, 2004), implying a weak San Andreas Fault (SAF) because the maximum compressive stress σ_1 is at a high angle to the San Andreas Fault.

We adopted the time-weakening friction law that allows a good resolution of the rupture breakdown process numerically (Andrews, 2004). The frictional parameters are chosen so that the dynamic stress drop is roughly 10% of the initial absolute normal stress on the fault. Because stress increases with depth the stress drop increases with depth as well. We simulate spontaneous ruptures under the simultaneous control of the assumed stresses and friction on the fault.

Figure 4 shows a rupture snapshot at 10 s on the fault for a rupture scenario that initiates at the intersection of the Sierra Madre and Cucamonga Faults. The hypocenter is 9 km deep. Both the nonplanar fault geometry and free surface cause time-dependent normal stress changes and affect rupture propagation significantly. The normal stress is more tensile after the rupture reaches the surface, which induces a larger stress drop – a feature typical of reverse faulting (e.g., Oglesby et al., 1998). The final slip distribution is shown in Figure 5, which indicates a strong rake rotation during rupture propagation. The moment magnitude of this rupture scenario is 7.7.

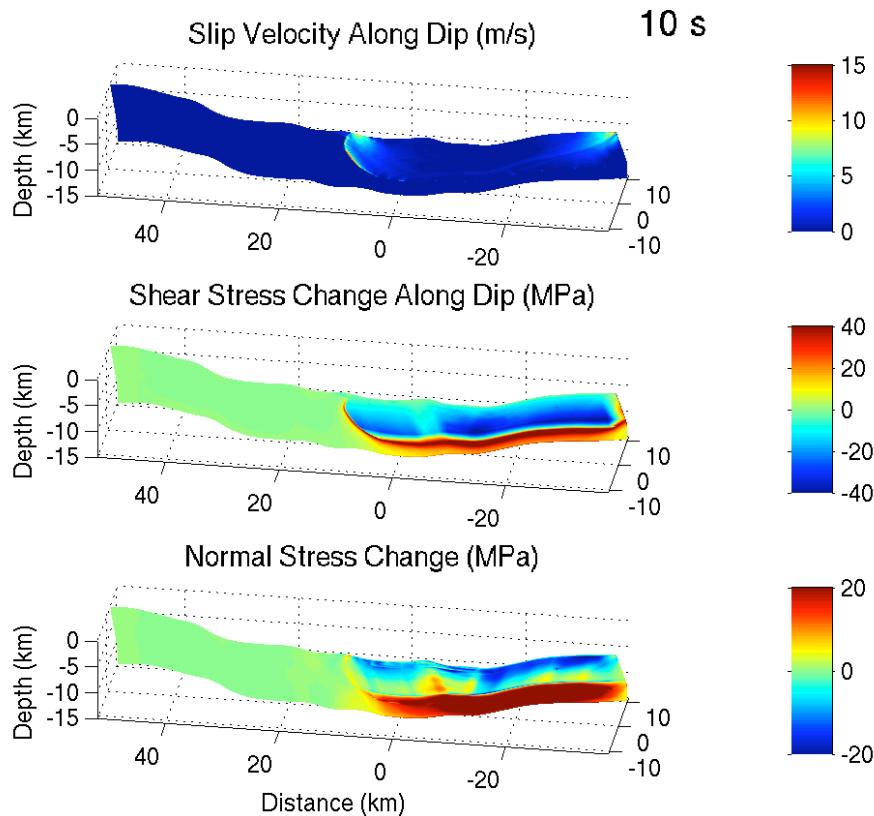


Figure 4. Rupture snapshot at 10 s are mapped on the fault. The hypocenter is 9 km deep and located approximately at $x = -20$ km. Both the nonplanar fault geometry and free surface have a significant effect on the rupture propagation.

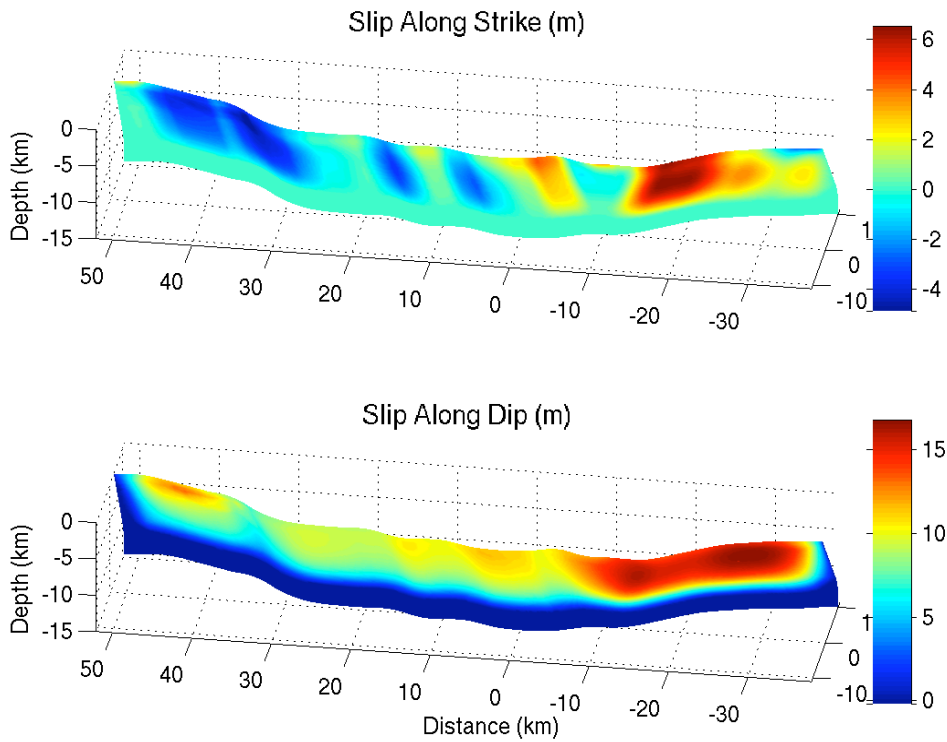


Figure 5. Two components of final slip are mapped on the fault, corresponding to M_w 7.7. Slip along strike is a significant fraction of total slip, indicating a strong rake rotation.

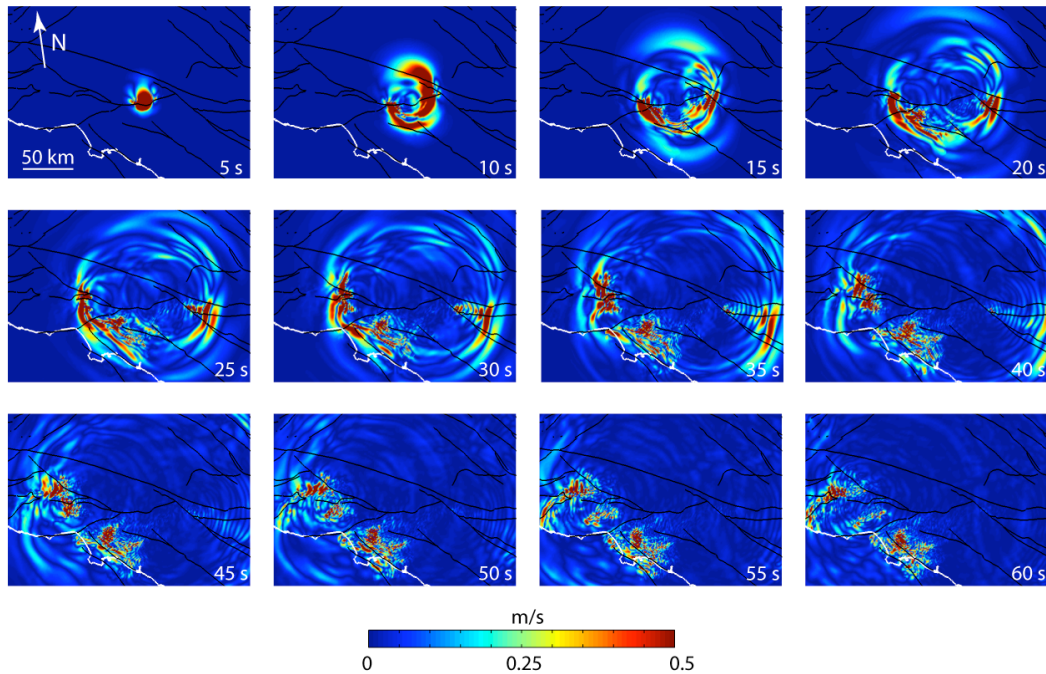


Figure 6. Snapshots of the amplitude of the ground velocity ($N8^\circ E$ component) due to an M_w 7.7 dynamic rupture scenario on the Sierra Madre – Cucamonga Fault system are mapped on the surface. Black lines depict major faults in the area. Color scale is saturated to better illustrate ground motion features. See text for details.

Figure 6 shows snapshots of ground velocity amplitude (N8°E component). The rupture propagates up-dip initially and large seismic energy is directed into the Los Angeles basin from the initial faulting. The basin velocity structure strongly affects the amplitude and duration of the ground motion in Los Angeles. The up-dip rupture terminates shortly and the rupture is thereafter dominated by the oblique motion as rupture propagates bilaterally. Large seismic waves propagate into the San Fernando Valley and Ventura Basin to the west and into the San Bernardino Basin to the east as well.

We show the three ground velocity components along a N8°E cross section (Figure 7). The velocity structure and fault geometry along the cross section is also shown. Ground motion in the Mojave region is mostly dominated by the source process, with relatively small amplitudes, as the velocity structure is relatively simple. In the Los Angeles basin, however, the seismograms show strong basin surface waves. Large ground velocity correlates well with basin depth. Large ground velocity can also be seen on the hanging wall (the San Gabriel Mountains), especially the vertical ground velocity.

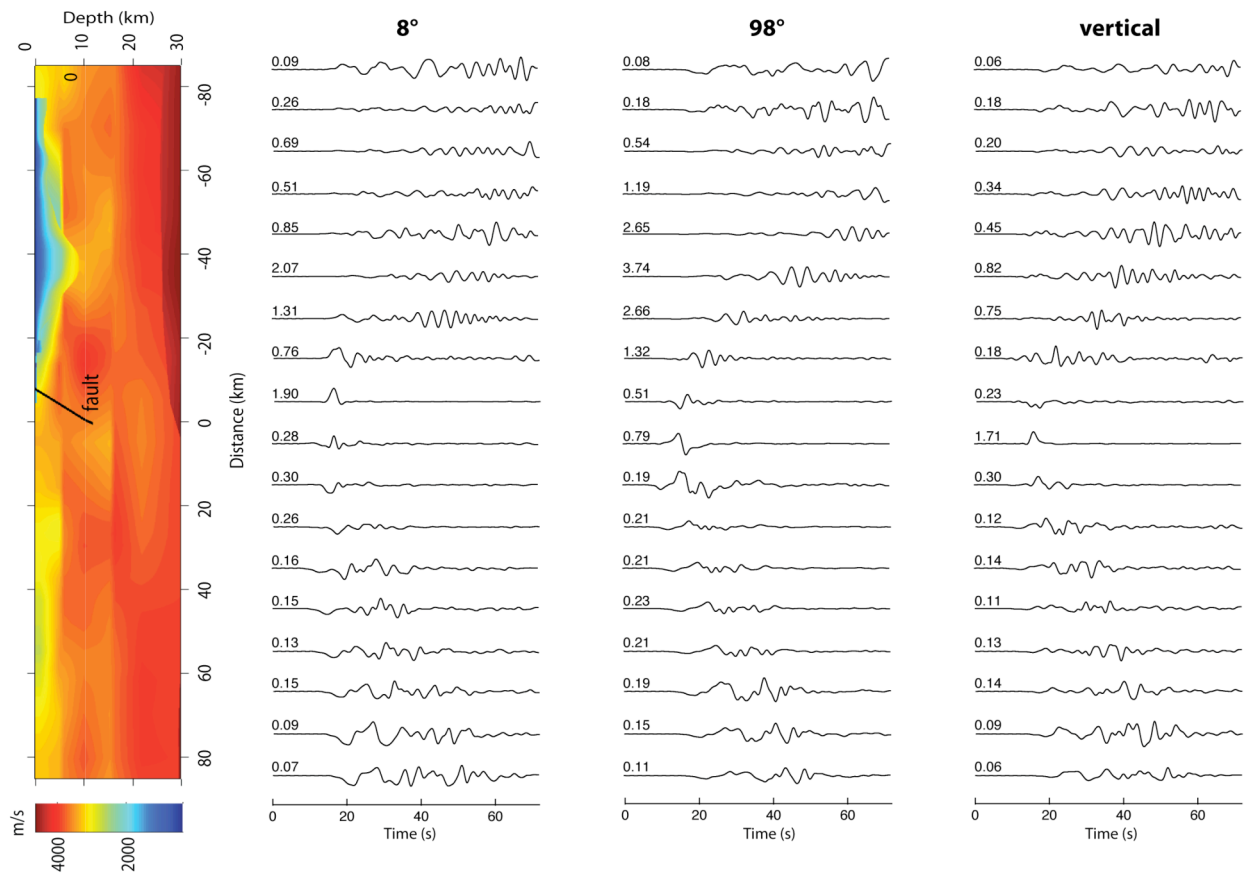


Figure 7. Three-component velocity time histories at surface along a cross section (N8°E) due to an M_w 7.7 dynamic rupture scenario on the Sierra Madre – Cucamonga Fault system. The S-wave velocity structure of the cross section is shown on the left. The peak amplitude of each time history (m/s) is indicated on each trace.

The peak ground velocity for this rupture scenario is illustrated in Figure 8a. Large ground motions are concentrated at distances very close to the fault as well as in the Los Angeles basin. The large vertical motion is mostly located in a narrow band (~10 km wide) on the hanging wall, where the peak ground velocity (PGV) reaches about 7 m/s. The large horizontal ground motion is, however, on the footwall. The distribution of PGV in the basin is very similar to one of the Terashake scenarios (Olsen et al., 2008) where the rupture propagates from southeast to the northwest on the SAF, which leads to the similar excitation of basins. The seismic energy (dominated by the basin surface waves) channels through the San Bernardino Valley, Chino Basin and Los Angeles Basin, resulting large amplification in certain areas where the ground motion reaches ~ 3 m/s. The velocity structure plays an important role in determining the ground motion levels. The robustness of the basin structure in these specific areas in the SCEC Community Velocity Model, however, needs to be validated with data. In the basin outside these specific areas, the ground velocity is in general less than 1 m/s, as clearly seen in the vertical component and one horizontal component (E8°S).

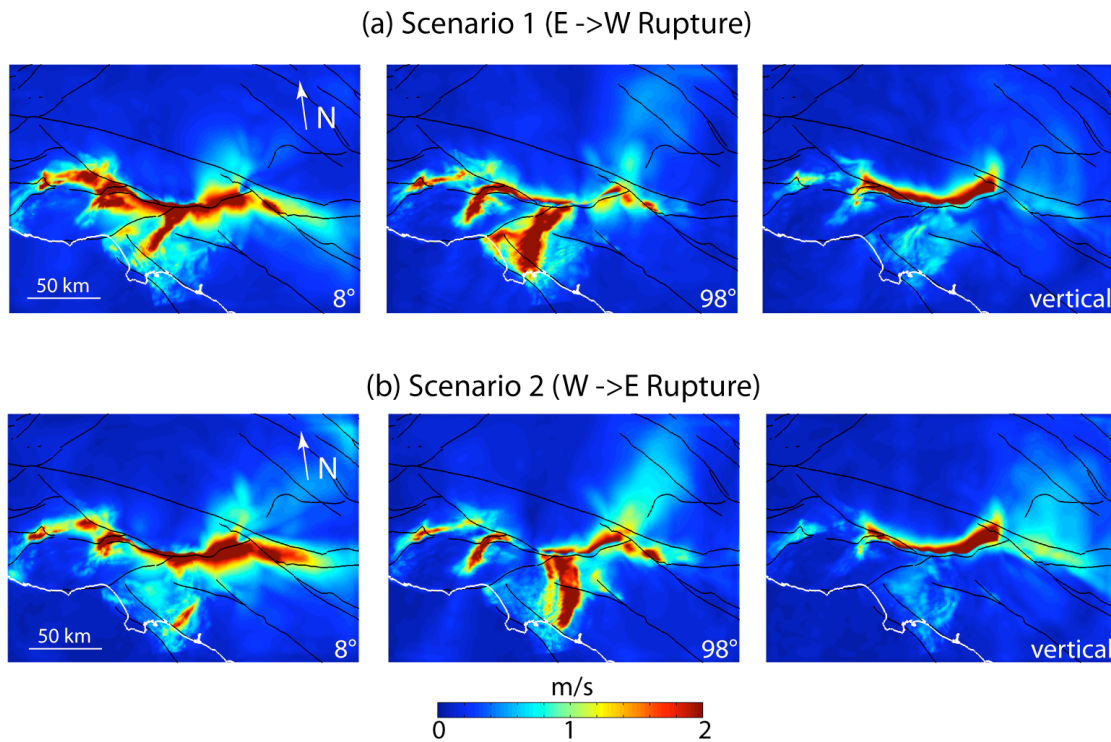


Figure 8. Distributions of PGV are mapped on the surface for two different rupture scenarios. Major faults in the area are shown in black lines. Large ground motions are located near the fault as well as in the Los Angeles basin. The color scale is saturated in order to better illustrate features. The large vertical ground motion is mostly located in a narrow band on the hanging wall where it reaches 7 m/s. The ground motion in the basin reaches 3 m/s in some specific areas, while it is in general less than 1 m/s outside these areas. The rupture directivity effect is not very strong.

A similar pattern is observed for a scenario where rupture propagates predominantly from the west to the east (Figure 8b). A similar level of ground motion is seen in the San Fernando Valley and San Bernardino Basin. This demonstrates that for this scenario, effects of the velocity structure are more important than source directivity. The relatively weak directivity effect is

attributable to the fact that the direction of rupture propagation (along strike) is not aligned with the slip direction (oblique slip) in large reverse earthquakes, as seen in the 1999 Chi-Chi earthquake (Aagaard et al., 2004). The amplification pattern in the Los Angeles basin is different as the excitation of the basin is different in these two rupture scenarios.

The up-dip directivity is also not very strong. The PGV in most areas in the basin is less than 1 m/s. The small up-dip directivity is due to the limited up-dip propagation distance. This is also consistent with the observation in the 2008 Wenchuan earthquake that the populated Sichuan basin did not suffer much damage even though it is located in the up-dip direction of the Longmen Shan Fault system.

The large ground motion on the hanging wall (Figure 8a, b) illustrates an important characteristic of ground motion during reverse faulting. Due to the broken symmetry of the dipping fault geometry with respect to the free surface, the free surface plays an important role in the rupture dynamics (e.g., Oglesby et al., 1998; O'Connell et al. 2007; Ma and Beroza, 2008). Wave reflections from the free surface interact strongly with evolving stress on the fault, and result in strongly time-dependent normal stress. In a homogeneous half space, for a reverse fault the normal stress ahead of rupture front is more compressive and more tensile behind it. This gives rise to a much larger strength drop (fault strength minus dynamic friction) near the surface, leading to much larger ground motion on the hanging wall than the footwall. Ma and Beroza (2008) considered a material contrast between hanging wall and footwall. They showed that the effect of material contrast can counteract the effect of free surface, somewhat, assuming that the hanging wall is less compliant as expected for crustal thrust faults. The SCEC Community Velocity Model does not show clear material contrast across the Sierra Madre – Cucamonga Fault system (Figure 5), however, so the bi-material effect is not an important factor in our simulations.

In summary, in the two elastic simulations of dynamic rupture simulation of M_w 7.7 events on the Sierra Madre – Cucamonga fault system, ground motion in the Los Angeles basin is in general less than 1 m/s, but in certain areas is as high as 3 m/s. Both up-dip and along-strike directivity is not particularly strong, as been observed in recent large thrust earthquakes such as the 1999 M_w 7.6 Chi-Chi earthquake and the 2008 M_w 7.9 Wenchuan earthquake. Ground motions, especially in the near field, will likely be reduced relative to those we have calculated, once we include the inelastic off-fault response (Andrews et al., 2007; Ma, 2008).

References:

- Aagaard, B. T., J. F. Hall, and T. H. Heaton, Effects of fault dip and slip rake angles on near-source ground motions: why rupture directivity was minimal in the 1999 Chi-Chi, Taiwan, earthquake, *Bull. Seismol. Soc. Am.*, **94**, 155-170, 2004.
- Andrews, D. J. (2004), Rupture models with dynamically determined breakdown displacement, *Bull. Seismol. Soc. Am.*, **94**, 769-775.
- Andrews, D. J., T. C. Hanks, and J. W. Whitney (2007), Physical limits on ground motion at Yucca Mountain, *Bull. Seismol. Soc. Am.*, **97**, 1771-1792.
- Dolan, J. F., K. Sieh, T. K. Rockwell, R. S. Yeats, J. Shaw, J. Suppe, G. J. Huftile, and E. M. Gath (1995), Prospects for larger or more frequent earthquakes in the Los Angeles metropolitan region, *Science*, **267**, 199-205.

- Harris, R. A., M. Barall, R. J. Archuleta, E. M. Dunham, B. Aagaard, J. P. Ampuero, H. Bhat, V. Cruz-Atienza, L. Dalguer, P. Dawson, S. Day, B. Duan, G. Ely, Y. Kaneko, Y. Kase, N. Lapusta, Y. Liu, S. Ma, D. Oglesby, K. Olsen, A. Pitarka, S. Song, E. Templeton (2009), The SCEC/USGS dynamic earthquake-rupture code verification exercise, *Seismol. Res. Lett.*, **80**, 119 – 126, doi: 10.1785/gssrl.80.1.119.
- Ma, S. and P. Liu (2006), Modelling of the perfectly matched layer absorbing boundaries and intrinsic attenuation in explicit finite-element methods, *Bull. Seismol. Soc. Am.*, **96**, 1779-1794, doi: 10.1785/0120050219.
- Ma, S., S. Custodio, R. J. Archuleta and P. Liu (2008), Dynamic modeling of the M_w 6.0 Parkfield, California, earthquake, *J. Geophys. Res.*, **113**, B02301, doi:10.1029/2007JB005216.
- Ma, S. and G. C. Beroza (2008), Rupture dynamics on a bi-material interface for dipping faults, *Bull. Seismol. Soc. Am.*, **98**, 1642 – 1658, doi: 10.1785/0120070201.
- Ma, S. (2008), A physical model for widespread near-surface and fault zone damage induced by earthquakes, *Geochem. Geophys. Geosyst.*, **9**, Q11009, doi:10.1029/2008GC002231.
- Magistrale, H., S. M. Day, R. W. Calyton, and R. Graves (2000), The SCEC southern California reference three-dimensional seismic velocity model version 2, *Bull. Seismol. Soc. Am.* **90**, S65-S76.
- Oglesby, D. D., R. J. Archuleta, and S. B. Nielsen (1998), Earthquakes on dipping faults: the effects of broken symmetry, *Science*, **280**, 1055–1059.
- Olsen, K. B., S. M. Day, J. B. Minster, Y. Cui, A. Chourasia, D. Okaya, P. Maechling, and T. Jordan (2008), TeraShake2: Spontaneous rupture simulations of M_w 7.7 earthquakes on the southern San Andreas Fault, *Bull. Seismol. Soc. Am.*, **98**, 1162-1185.
- Plesch, A. and others (2007), Community Fault Model (CFM) for southern California, *Bull. Seismol. Soc. Am.*, **97**, 1793-1802.
- Rubin, C. M., Lindvall, S., and Rockwell, T. (1998), Paleoseismic evidence for large slip earthquakes along the Sierra Madre fault in the greater Los Angeles region, *Science*, **281**, 398-402.